Influence of electron density and trion formation on the phase-coherent photorefractive effect in ZnSe quantum wells

A. Kabir and H. P. Wagner
Department of Physics, University of Cincinnati, Cincinnati, Ohio 45221-0011, USA
(Received 7 December 2010; revised manuscript received 19 January 2011; published 18 March 2011)

We investigate the influence of electron density and trion formation on the phase-coherent photorefractive effect in ZnSe single quantum wells by laser energy and temperature dependent degenerate four-wave-mixing experiments using 90-fs pulses. Two different structures with the same quantum well width and confinement energy but different barriers adjacent to the GaAs substrate are studied in order to compare the formation of a photorefractive electron density grating at specific excitation conditions. At temperatures below 35 K and laser excitation energy close to the exciton energy the formation of trions significantly suppresses the generation of an electron density grating. At lower excitation energies increasing space-charge fields reduce the trion binding energy which leads to an enhanced thermal ionization of trions resulting in a strong phase-coherent photorefractive effect. Due to the thermal dissociation of trions at temperatures exceeding 45 K a significant photorefractive effect exists even at exciton resonant excitation. The experimentally observed signal traces obtained at different excitation conditions are in good agreement with model calculations that are based on the optical Bloch equations, including inhomogeneous broadening at strong space-charge fields.

DOI: 10.1103/PhysRevB.83.125305 PACS number(s): 78.67.De, 71.55.Gs, 71.35.−y, 42.50.Md

I. INTRODUCTION

Controlled carrier transfer between heterovalent structures involving II-VI and III-V semiconductor compounds has recently attracted attention because of possible applications in spintronics[1–4] and photovoltaics.[5–7] Based on such carrier transfer, we recently discovered a phase-coherent photorefractive (PCP) effect in ZnSe/ZnMgSe quantum wells (QWs) grown on (001) GaAs using 90-fs light pulses in a two-beam four-wave mixing (FWM) configuration with light energies resonant to QW excitons.[8,9] The observed photorefractive effect is caused by the creation of a spatially modulated electron density in the QW in a multistep process: A fraction of the exciting light pulses with 2.81 eV center energy and noncollinear wave vectors $\mathbf{k}_1$ and $\mathbf{k}_2$ is used to create an exciton density grating by the interference of coherent excitons in the QW. The remaining pulse energy is used to create electron–hole pairs in the GaAs substrate (with a band-gap energy of ∼1.48 eV at 10 K). The valence band offset (>0.6 eV) between the ZnMgSe barrier and the GaAs substrate[10,11] prevents holes from crossing the heterovalent interface but the conduction-band offset allows electrons to pass the interface after interacting with phonons in the GaAs substrate.[12–17] After cooling with phonons in the II–VI materials[18–22] these electrons are captured in the ZnSe QW within a total transfer time of ∼30 ps, as recently observed in three-beam FWM experiments.[23] Due to the repulsive interaction (Coulomb interaction and Pauli blocking) with the exciton density grating in the QW a long living (∼10 μs) π-shifted electron grating is formed, which is stabilized by localized holes at the barrier/GaAs interface.[8,9] The spatially modulated electron density in the QW and corresponding hole grating at the interface create space-charge fields, which are responsible for the occurrence of the photorefractive effect.

The high diffraction efficiency of this PCP effect (∼0.1%) and the long electron grating lifetime bear tremendous potential for optical data storage and real-time holographic imaging. Unlike in other photorefractive QW devices,[24–26] PCP QWs operate without electrical contacts providing large working areas for holographic imaging and avoiding device degradation due to Joule heating. Furthermore, the PCP effect utilizes the coherence of excitons for time gating. As has been recently demonstrated,[27,28] this time gating enables the acquisition of single-shot three-dimensional (3D) holographic images of still and moving objects. However, for an improvement of PCP QW structures a better understanding of the physical processes that lead to the formation of a spatially modulated electron density is necessary. In this paper we investigate the influence of the captured electron density and the formation of trions on the PCP effect by performing laser energy and temperature dependent degenerate FWM experiments. Two samples with the same QW width and confinement energy but different barrier structure and barrier width are studied. The experimentally observed signal traces are compared with model calculations that are based on the optical Bloch equation, including field-induced inhomogeneous broadening at strong space-charge fields.

II. EXPERIMENTAL DETAILS

The investigated ZnSe single QWs (SQWs) were pseudomorphically grown on (001) oriented GaAs substrate by molecular beam epitaxy.[29] QW1 (which refers to sample C in Ref. 30) consists of a 10-nm-wide ZnSe SQW sandwiched between a 30-nm-thick $Zn_{0.90}Mg_{0.10}Se$ top barrier and a 20-nm-thick $Zn_{0.90}Mg_{0.10}Se$ bottom barrier. QW2 (which refers to sample A in Ref. 30) consists of a 10-nm-wide ZnSe SQW sandwiched between two 30-nm $Zn_{0.90}Mg_{0.10}Se$ barriers, with a 20-nm-thick ZnSe buffer layer between the barrier and the GaAs substrate. Because of the different distance between the QW and the GaAs substrate we expect a reduced captured equilibrium electron density n_e in QW2 compared to QW1 as we conclude from earlier FWM measurements

where the trion signal is significantly reduced in QW2.[30] In addition, due to the presence of the buffer layer in QW2 we expect a reduced density of dislocations within the barrier at which electrons can be trapped that reduce the space-charge field between the QW and the GaAs substrate. The differences of the captured electron density and density of dislocations motivated us to study and compare the PCP effect in these two samples.

A frequency doubled mode-locked Ti-sapphire laser providing ultrashort pulses of a spectral width of 22 meV at a repetition rate of 80 MHz was used to excite the sample. The temporal width of the frequency doubled pulses was determined to 90 ± 5 fs using an autocorrelation technique that is based on the two-photon absorption in a SiC photodiode. For the excitation energy dependent measurements the laser energy has been stepwise shifted with an accuracy of ±0.7 meV. Two-beam four-wave-mixing (FWM) experiments with collinear polarized pulses $\mathbf{k}_1$ and $\mathbf{k}_2$ and mutual delay τ have been performed in backscattering geometry with the sample mounted in a closed cycle cryostat at temperatures between 12 and 75 K. The zero delay between different pulses has been determined by the contrast of the interference pattern appearing on the sample surface during the temporal overlap of the pulses. The $1/e^2$ focus diameter of the laser pulses on the sample was ∼100 μm. The time integrated and spectrally resolved four-wave-mixing signal was detected into direction $2\mathbf{k}_2 - \mathbf{k}_1$ by a combination of a spectrometer and an optical multichannel analyzer.

III. EXPERIMENTAL RESULTS AND DISCUSSION

A. Laser energy dependent measurements

Figure 1 shows the normalized signal traces at the spectral position of the X_h heavy-hole exciton transition in the $2\mathbf{k}_2 - \mathbf{k}_1$ direction of QW1 as a function of delay τ at a temperature of 20 K for different excitation energies as labeled. For better visibility the traces have been offset with respect to each other and the signal intensity is given on a logarithmic scale. The total excitation intensity of pulses $\mathbf{k}_1$ and $\mathbf{k}_2$ was 40 kW cm^{-2} in these experiments (corresponding to a total average power of 24 μW). In the top trace the center energy of the excitation pulses was set resonant to the X_h heavy-hole exciton transition energy (∼2.8115 eV). At this excitation energy and for decreasing pulse energies down to ∼2.800 eV we find a pronounced signal spike at pulse overlap (PO signal)[9] which is attributed to a photorefractive effect caused by a spatially modulated electron density that has been transferred from the GaAs substrate to the ZnSe QW. Longitudinal space-charge fields between captured QW electrons and localized holes at the ZnMgSe barrier/GaAs interface cause a periodic modulation of the optical constants according to the quantum confined Stark effect (QCSE) resulting in a diffracted exciton polarization into direction $2\mathbf{k}_2 - \mathbf{k}_1$. Besides this strong PO signal the traces reveal a weak $\chi^{(3)}$ FWM signal for positive delay $\tau > 0$ (pulse $\mathbf{k}_2$ arrives last) exhibiting a small modulation at ∼1.3 ps. This modulation is caused by the interference of excitons X_h with coherent trions T being weakly visible at 2.8 meV lower energy[30] with respect to the X_h line in the normalized diffracted signal spectra at pulse overlap, as displayed in Fig. 2. The signal spectra are offset with respect to each other for better visibility. During the laser energy shift of negative 11 meV with respect to the resonantly excited X_h transition energy the exciton line exhibits a redshift of 0.9 meV with increasingly weaker trion contribution. The exciton dephasing rate γ_2 extracted from the signal traces (assuming nearly homogeneous broadening of the exciton line at these excitation conditions) remains almost constant (∼0.8 ps^{-1}) for laser shifts below 6.5 meV but increases for higher energy shifts showing a rate of $\gamma_2 \sim 1$ ps^{-1} at an excitation of 2.800 eV.

For laser excitations below 2.798 eV the signal traces as well as the observed redshift and exciton dephasing rates suddenly change. In contrast to the observed signal peak below a critical X_h redshift of 1.9 meV the signal trace exhibits a signal dip at pulse overlap and a PCP signal trace with almost symmetric decay for positive and negative pulse delay appears (see Fig. 1). (The slightly higher signal at

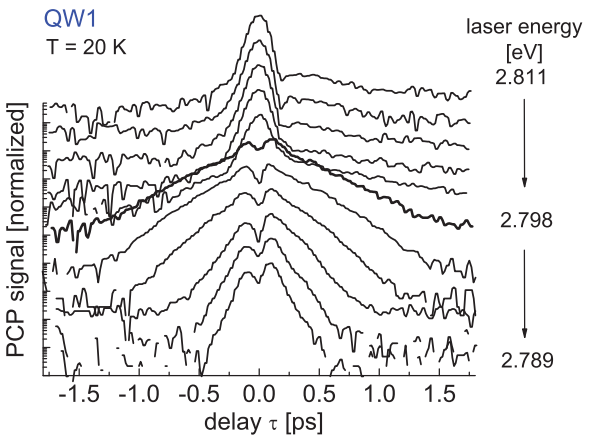

FIG. 1. (Color online) Normalized signal traces at the X_h heavy-hole exciton of QW1 as a function of delay τ on a logarithmic scale at a temperature of 20 K for different excitation energies as labeled. For better visibility the traces have been offset with respect to each other.

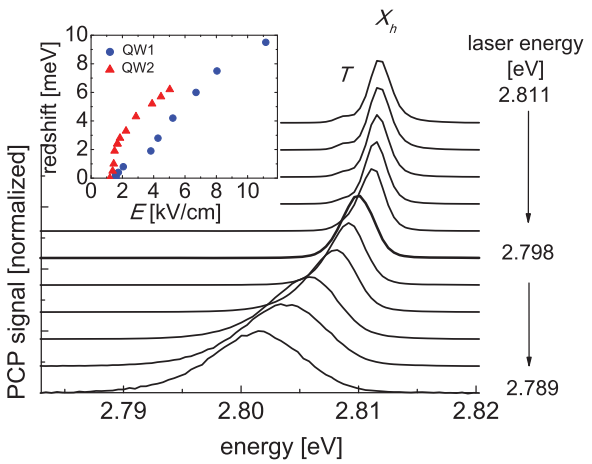

FIG. 2. (Color online) Normalized signal spectra of QW1 at a temperature of 20 K for different excitation energies as labeled. For better visibility the traces have been offset with respect to each other. The inset shows the energy shift of the exciton position of QW1 (full blue circles) and QW2 (full red triangles) as a function of the space-charge field as described in the text.

positive delay is caused by the additional weak $\chi^{(3)}$ FWM signal.) As explained,[8,9] this PCP signal is caused by the formation of a long-living electron grating that is induced by the repulsive Coulomb interaction and Pauli blocking of the spatially modulated exciton density in the QW. The PCP electron grating is π shifted with respect to the electron grating at pulse overlap leading to a signal suppression within the pulse autocorrelation time.[8,9] Like for the PO signal, longitudinal space-charge fields cause a diffraction of the exciton polarization into direction $2\mathbf{k}_2 - \mathbf{k}_1$, however, since the exciton grating amplitude decreases proportional to $\exp(-\tau\gamma_2)$ the signal intensity decays with a rate of $2\gamma_2$ for negative ($\tau < 0$) and positive delay times ($\tau > 0$). With decreasing pulse energy the signal trace reveals a nonexponential decay as a function of delay τ and the spectral width of the exciton line X_h considerably broadens. As explained in Sec. III C the observed increasing decay rate and spectral broadening is attributed to a space-charge field-induced inhomogeneous broadening of exciton energies. The spectral shift of the maximum position of the X_h signal intensity as a function of the laser energy shift (with initial laser energy being resonant to the X_h transition) is summarized as full blue circles in Fig. 3. The accuracy of the stepwise shifted laser energy is ± 0.7 meV as indicated by the error bar in the leftmost data point.

The observed behavior of the diffracted signal as a function of the laser energy can be explained by the formation of trions which significantly compensates the generation of a photorefractive electron grating in the QW at nearly exciton resonant excitation. Accordingly, the diffracted signal at time delays beyond pulse overlap merely shows a weak $\chi^{(3)}$ four-wave-mixing signal at positive delay $\tau > 0$. At pulse overlap transferring substrate electrons enter the QW as spatially modulated electron density and the diffracted signal is

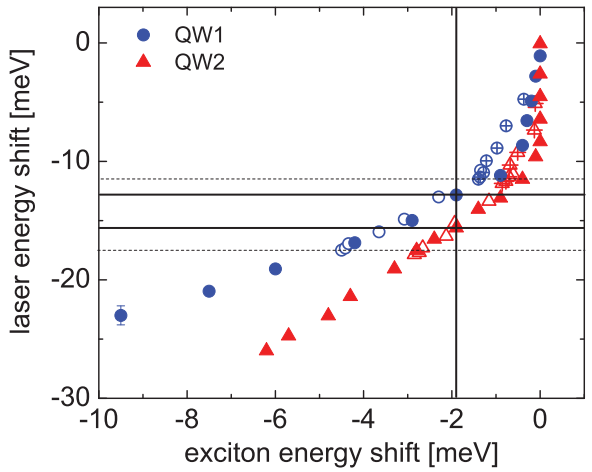

FIG. 3. (Color online) Spectral shift of the X_h signal as a function of the laser energy shift in QW1 (full blue circles) and in QW2 (full red triangles). The crossing points of the full horizontal lines and vertical line indicate the transition from the PO to the PCP effect at a critical exciton redshift of 1.9 meV. The dashed horizontal lines indicate the laser energies, which are used in the temperature-dependent measurements. Open and open-crossed circles and triangles show the extracted exciton redshift of QW1 and QW2, respectively, as a function of the laser energy difference obtained from temperature-dependent FWM measurements.

predominantly caused by a strong PO effect. With decreasing laser energy the density of excited QW excitons decreases, which results in a reduced phase-space filling of electron states and lowered electron escape rate of captured substrate electrons in the QW due to Auger processes of recombining excitons.[9] Both effects increase the equilibrium density n_e of captured electrons in the QW. The enhanced electron density n_e causes a stronger static electric field E between the QW electrons and holes at the barrier/substrate interface shifting the exciton line towards lower energy. The E-field-induced tilt and deformation of the QW band energies also separates the electron and hole wave functions of trions in the QW leading to a decrease of the trion binding energy,[31,32] which in turn increases the probability of thermal trion ionization at 20 K. At a laser energy of 2.798 eV the generated electric field E reaches a critical value at which the formation of trions is significantly suppressed. Repulsive forces between excitons and captured electrons start to dominate resulting in a π-shifted PCP electron grating in the QW. Further reduction of the laser energy increases the electron density n_e, which leads to an increasing redshift of the exciton line as well as to faster exciton dephasing due to enhanced exciton-electron scattering rates.

This interpretation is supported by FWM experiments with pulse intensities of 5 MW/cm^2 at 12 K where trions are thermally more stable. Figure 4 shows the FWM spectra of coherent trions (T) and excitons (X_h) at pulse overlap as a function of the exciting laser energy as labeled. Above an excitation energy of 2.798 eV the FWM signal intensity of excitons and trions are comparable but the trion binding energy decreases from 2.8 to $\sim$1.6 meV resulting in a smaller total linewidth of the combined exciton/trion band. Below 2.798 eV the trion signal significantly decreases because of thermal ionization at further reduced trion binding energy and the onset of the PCP effect.

To estimate the electron density n_e at a given laser energy as well as the resulting critical electric field E, which is responsible for the trion suppression, we recall that an increased electron density leads to an enhanced exciton-electron

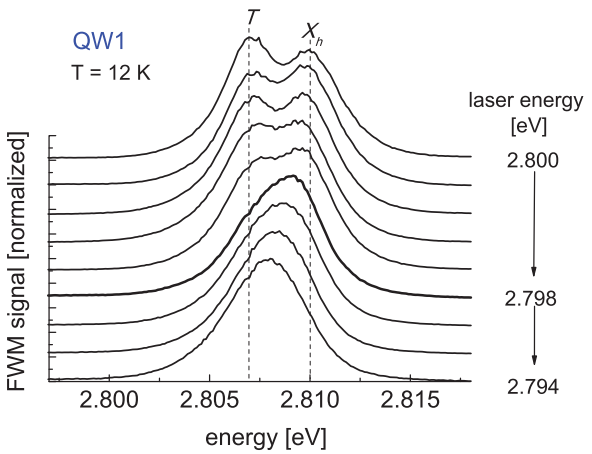

FIG. 4. (Color online) FWM spectra of coherent trions (T) and excitons (X_h) at a temperature of 12 K as a function of the exciting laser energy as labeled. The vertical lines are guides for the eye.

scattering which increases the exciton dephasing rate γ_2 according to

$$\gamma_2(n_X,n_e,T) = \gamma_2(n_X,T) + \beta_{Xe} n_e. \quad (1)$$

In Eq. (1) β_{Xe} is the electron-exciton scattering rate and $\gamma_2(n_X,T)$ is the dephasing rate due to exciton-exciton scattering[33] and scattering with acoustic and LO phonons at a given temperature T.[34–36] $\gamma_2(n_X,T)$ further includes a background dephasing rate γ_{20} due to crystal imperfections. At low excitation energies we assume nearly homogeneous broadening of the X_h exciton line. Neglecting $\gamma_2(n_X,T)$ for low exciton densities n_X and low temperature (20 K) and further assuming $\gamma_{20} \approx 0$ we estimate an upper limit of the electron density to $n_e \approx 1.9 \times 10^{10}$ cm^{-2} at ~2.798 eV (where the conversion from the PO spike to the PCP signal takes place) using an exciton-electron scattering rate of $\beta_{Xe} \approx 100$ s^{-1}cm^2.[37] At lower excitation energies the trace of the PCP signal becomes nonexponential due to E-field-induced inhomogeneities within the QW structure. Accordingly, the exciton dephasing rates γ_2 have been extracted considering a Gaussian distribution of exciton energies (as described in Sec. III C) providing an electron density of $n_e \approx 5.5 \times 10^{10}$ cm^{-2} at the lowest excitation energy.

The static space-charge field E between QW electrons and holes at the barrier/substrate interface is estimated by $E = \sigma/(\varepsilon\varepsilon_0)$ with a surface charge density $\sigma = n_e e$, with e being the electron charge and static dielectric constant $\varepsilon = 9$ assuming no electron trapping in the barrier due to crystal imperfections. The inset in Fig. 2 shows the observed redshift of the exciton line as a function of the built-in electric field E. The exciton redshift shows a sudden increase when the electric field E reaches a critical value of $E \approx 3.8 \times 10^3$ V cm^{-1} being responsible for the suppression of the trion formation. Different from the expected quadratic dependence in QCSE we observe a sublinear dependence of the exciton redshift at higher fields. We attribute this behavior to the fact that the space-charge fields end in the PCP QW instead of passing the QW structure as in externally biased photorefractive devices.[24–26] Furthermore, the saturation of the exciton redshift is attributed to an increasing repulsive electric potential for electrons passing the barrier and to enhanced electron grating diffusion at high electron densities.

For comparison we also performed laser-dependent measurements on QW2 at 20 K using the same excitation intensities as for QW1. Due to the larger barrier width we expect a reduced equilibrium electron density n_e compared to QW1 which is supported by a significantly reduced trion signal in earlier FWM measurements[30] and no observable coherent trion spectrum using a total intensity of 40 kWcm^{-2} in these experiments (not shown). The general behavior of the signal trace obtained from QW2 is similar to that observed in QW1. At laser energies close to the exciton X_h resonance (at ~2.812 eV) we observe a PO signal spike and a combination of a weak PCP and FWM signal for delays beyond $\tau \approx 0$ (compare Fig. 5 at 20 K). However, since the equilibrium electron density n_e is reduced compared to QW1 we observe a decreased redshift of the X_h line in QW2 at comparable laser energies. Accordingly, the laser energy needs to be shifted to ~2.796 eV (2 meV lower as compared to QW1) to achieve

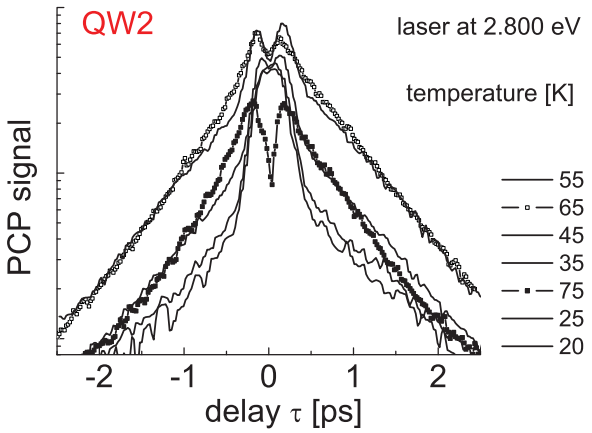

FIG. 5. (Color online) Signal traces at the spectral position of the X_h heavy-hole exciton of QW2 as a function of delay τ on a logarithmic scale at temperatures ranging from 20 to 75 K. The exciting laser energy was 2.800 eV.

a 1.9 meV shift of the exciton line to lower energy where we find a sudden increase of the PCP signal indicating the suppression of trion formation. Further decrease of the laser energy leads to an additional redshift of the X_h line and an increase of the exciton dephasing rate. The shift of the exciton line X_h with respect to the laser energy shift is shown in Fig. 3 as full red triangles. The X_h shift as a function of the E field generated by captured QW electrons n_e is given in the inset of Fig. 2. As in QW1 the dephasing rate γ_2 has been extracted from the signal decay including inhomogeneous broadening at higher space-charge fields. Different than QW1, the critical exciton redshift of 1.9 meV already occurs at an electric field of $E \approx 1.5 \times 10^3$ V cm^{-1}. The reduced value of the critical E field compared to QW1 is attributed to the insertion of a buffer layer in sample QW2, which reduces the density of dislocations within the barrier[29] at which electrons can be trapped.

B. Temperature dependent measurements

To support our interpretation we further performed temperature dependent FWM measurements at fixed laser energies. The laser energies were chosen to be 2.800 eV where trion formation is present, and 2.794 eV where it is suppressed in both samples (compare dashed lines in Fig. 3). Figure 5 shows the signal traces on a logarithmic scale obtained from QW2 for temperatures ranging from 20 to 75 K at 2.800 eV laser energy and 40 kW cm^{-2} excitation intensity of pulses $\mathbf{k}_1$ and $\mathbf{k}_2$. As expected, we find a signal spike at pulse overlap and a combination of a weak $\chi^{(3)}$ FWM and PCP signal at delays beyond pulse autocorrelation at 20 K. The contribution of the PCP signal increases with increasing temperature leading to the occurrence of a dip within the PO signal at 35 K and reaching a PCP signal maximum at ~55 K. Above this temperature the PCP signal starts to decrease, which is attributed to an increased thermal diffusion of the exciton density grating during the electron grating formation and enhanced phonon-assisted tunneling of electrons back to the GaAs substrate,[38,39] resulting in a reduced spatial modulation of the space-charge fields in the QW structure. The spectral

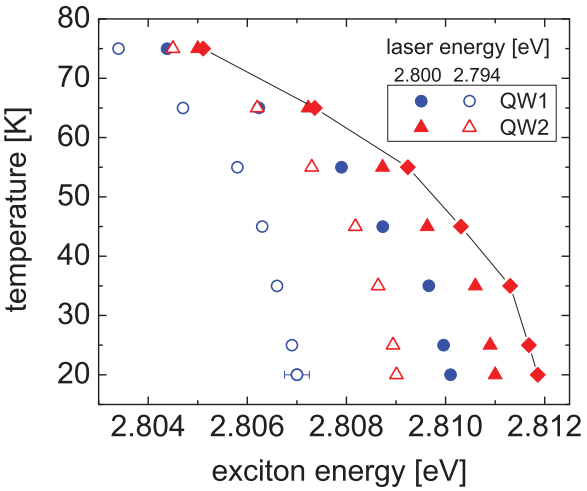

FIG. 6. (Color online) Spectral shift of the X_h heavy-hole exciton line as a function of temperature for samples QW1 and QW2 at excitation energies 2.800 eV (full blue circles and red triangles, respectively) and at 2.794 eV (open blue circles and red triangles, respectively). For comparison the X_h shift in QW2 obtained from FWM experiments at resonant excitation is shown as full red diamonds.

shift of the X_h line as a function of temperature, shown as red triangles in Fig. 6, is caused by both band-gap shrinkage and E-field-induced redshift due to the captured electron density n_e. The accuracy of the determined exciton energy is ± 0.3 meV as indicated by the error bar in the leftmost data point at 20 K.

With increasing temperature the energy difference between the fixed laser energy and exciton transition energy X_h decreases, therefore the electron density n_e and E-field-induced redshift of the X_h line diminishes. In order to discriminate the E-field-induced exciton redshift from the band-gap shrinkage the exciton line shift obtained from FWM experiments at resonant X_h excitation is shown as red diamonds for comparison. Open crossed red triangles show the measured exciton redshift as a function of the laser energy distance with respect to the exciton energy due to band-gap shrinkage. The reduced redshift of the exciton line as a function of the reduced laser energy distance at higher temperatures agrees with the results obtained from laser energy dependent measurements. Deviations are attributed to a slightly higher electron capture rate at higher temperature causing an enhanced redshift due to an increased equilibrium density n_e. Figure 7 displays the exciton dephasing rate $\gamma_{Xe} = \beta_{Xe} n_e$ caused by exciton-electron scattering and the extracted electric field E as a function of temperature using Eq. (1) and subtracting the contribution of phonon scattering.[34–36] In these calculations we assume nearly homogeneous broadening of the X_h exciton. Despite the reduced electron density n_e and decreased space-charge fields favoring the formation of trions, the PO signal conforms into a PCP signal at ~45 K due to the increasing thermal dissociation of trions at higher temperature.

The temperature-dependent traces at 2.800 eV excitation energy of QW1 (not shown) look very similar to the traces obtained from QW2. At 20 K the contribution of PCP is smaller so that the signal at $\tau > 0$ is merely due to $\chi^{(3)}$ FWM (compare Fig. 1) which is attributed to the higher equilibrium electron

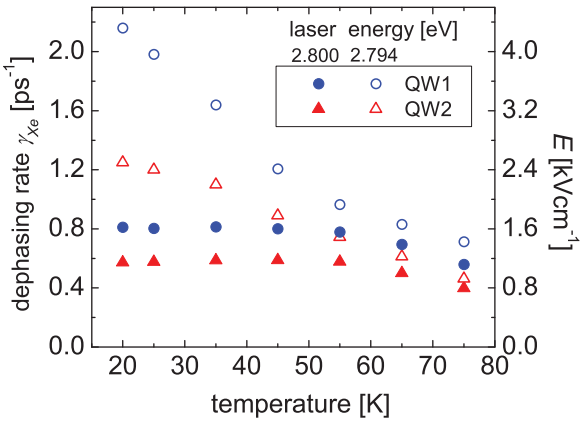

FIG. 7. (Color online) Exciton dephasing rate γ_{Xe} caused by exciton-electron scattering and extracted electric field E as a function of temperature for QW1 and QW2 at excitation energies 2.800 eV (full blue circles and red triangles, respectively) and at 2.794 eV (open blue circles and red triangles, respectively).

density n_e in QW1 leading to a stronger suppression of the PCP signal due to trion formation. At 35 K the PCP contribution starts to increase and becomes the dominant process above 45 K. The spectral shift of the X_h line is depicted as full blue circles in Fig. 6 and the extracted exciton redshift as a function of the laser energy distance is shown as open crossed blue circles in Fig. 3. Due to the higher electron concentration n_e at 20 K the X_h redshift in QW1 is more pronounced as in QW2. The extracted electron dephasing γ_{Xe} (assuming nearly homogeneous broadening at this excitation condition) and calculated electric field E are shown in Fig. 7 as full blue circles. As in QW2, the transition from the PO signal into a PCP signal is explained by the increasing thermal dissociation of trions with rising temperature.

At lower excitation energy (2.794 eV) the increased electron density n_e and resulting electric field E strongly suppress the formation of trions so that even at 20 K, PCP is the dominating effect in both QW structures. Figure 8 shows the traces of QW1 at temperatures ranging from 20 to 75 K. Since the electron density n_e is highest at 20 K, the spectral position of X_h is

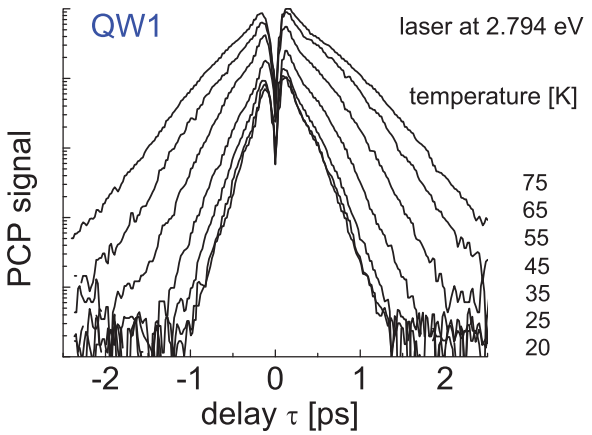

FIG. 8. (Color online) Signal traces at the X_h heavy-hole exciton of QW1 as a function of delay τ on a logarithmic scale at temperatures ranging from 20 to 75 K. The exciting laser energy was 2.794 eV.

shifted most with respect to its position at resonant excitation, as demonstrated in Fig. 6 and in Fig. 3 as open blue circles and open red triangles for QW1 and QW2, respectively. As mentioned earlier, the traces given on a logarithmic scale do not show a linear dependence but show a nonlinear decay as a function of delay τ which is attributed to an E-field-induced inhomogeneous broadening of the X_h transition energies at high space-charge fields. Accordingly, the exciton dephasing rates γ_2 have been extracted from the experimental signal traces and spectra considering inhomogeneous broadening as described in the following section. Figure 7 summarizes the extracted exciton dephasing rates γ_{Xe} and electric-field values at an excitation energy of 2.794 eV for both samples. Both the measured exciton redshift (compare Fig. 3) and extracted E-fields are consistent with the results obtained from laser energy dependent measurements confirming the importance of trion formation and the influence of the electron density on the occurrence of the PCP effect.

C. Modeling of the signal traces

For nearly exciton resonant laser energies, which correspond to a low captured electron density n_e and low space-charge fields, the diffracted polarization $\boldsymbol{P}_D(\omega,\tau)$ into direction $2\mathbf{k}_2-\mathbf{k}_1$ is modeled using the optical Bloch equations (OBE) of a homogeneously broadened two-level system for δ-shaped collinearly polarized laser pulses. Small contributions due to $\chi^{(3)}$ FWM from excitons and trions have been neglected. After Fourier transformation the diffracted polarization $\boldsymbol{P}_D(\omega,\tau)$ reads

$$\begin{aligned}\boldsymbol{P}_D(\omega,\tau) &= a\boldsymbol{P}_{PCP}(\omega,\tau) - b\boldsymbol{P}_{PO}(\omega,\tau)\\ &\propto \left[a_{\mathbf{k}_2-\mathbf{k}_1}(\tau) - b_{\mathbf{k}_2-\mathbf{k}_1}(\tau)\right]\boldsymbol{P}_{\mathbf{k}_2}(\omega,\tau).\end{aligned} \tag{2}$$

In Eq. (2) the function

$$\boldsymbol{P}_{\mathbf{k}_2}(\omega,\tau) \propto -\frac{1}{\hbar}\frac{\mu_{21}^2}{(\omega-\Omega_{21})}\exp(i\omega\tau)$$

describes the exciton polarization into direction $\mathbf{k}_2$ and $a_{\mathbf{k}_2-\mathbf{k}_1}(\tau)$ is proportional but π-shifted to the exciton density grating that is responsible for the subsequent formation of a PCP electron grating in regions of low exciton density, given by

$$a_{\mathbf{k}_2-\mathbf{k}_1}(\tau) = a\theta(-\tau)\,\mu_{21}^2\exp(i\Omega_{21}\tau) + a\theta(\tau)\,\mu_{21}^2\exp(i\Omega_{21}^*\tau). \tag{3}$$

In Eq. (3) μ_{21} accounts for the magnitude of the dipole transitions and $\Omega_{21}=\omega_{21}-i\gamma_2$ contains the angular frequency ω_{21} between ground state $|1\rangle$ and excited level $|2\rangle$ and the exciton dephasing rate γ_2 as given in Eq. (1). The empirical parameter a accounts for the contribution of the PCP polarization to the total diffracted polarization.

Function $b_{\mathbf{k}_2-\mathbf{k}_1}(\tau)$ in Eq. (2) describes the electron-density grating that is created during pulse overlap and is given by

$$b_{\mathbf{k}_2-\mathbf{k}_1}(\tau) = b\exp(i\omega_p\tau)\left[\int E_{\mathbf{k}_2}(t-\tau)E_{\mathbf{k}_1}(t)\,dt\right]. \tag{4}$$

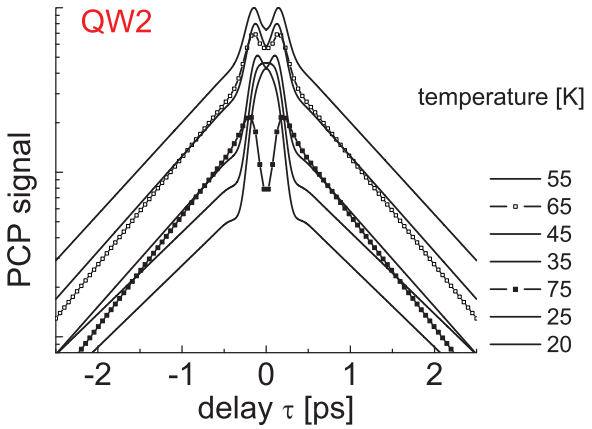

FIG. 9. (Color online) Calculated traces at the spectral position of the X_h heavy-hole exciton in sample QW2 as a function of delay τ at an excitation energy of 2.800 eV and at temperatures ranging from 20 to 75 K using Eqs. (2)–(4). Nearly homogenously broadened exciton transitions have been assumed at this excitation condition.

In Eq. (4) the integral gives the field autocorrelation of sech(t)-shaped pulses with temporal full width at half maximum (FWHM) of $1.49\Delta t$ where Δt is the measured FWHM of the incident laser pulse intensity. ω_p is the center frequency of the pulse and parameter b is a measure of the contribution of the PO polarization at $\tau\approx 0$. The minus sign of parameter b in Eq. (2) considers the π-shift of the electron grating at pulse overlap with respect to the PCP electron grating.

Figure 9 demonstrates the calculated traces of QW2 for different temperatures and excitation energy of 2.800 eV using Eqs. (2)–(4) where the dephasing rates γ_2 of the nearly homogenously broadened exciton transition were extracted from the experimental traces shown in Fig. 5 and the spectral positions ω_{21} of the X_h transition were taken from Fig. 6. For the temporal FWHM of the excitation pulses we applied $\Delta t = 90$ fs, and parameters a and b were adjusted to fit the experimental data. The calculated traces are in good agreement with the experimentally observed exciton traces at different temperatures (compare Fig. 5).

While the assumption of homogeneous exciton broadening is appropriate for low electron densities n_e, the intrinsic inhomogeneous broadening of X_h energies due to QW fluctuations increases at high electric fields due to varying Stark shifts at different QW widths. Electric-field fluctuations due to crystal imperfections at the GaAs interface may also contribute to this field-induced broadening. Modifications of the broadening due to the spatial modulation of the space-charge field, which is a function of the delay τ between pulses $\mathbf{k}_1$ and $\mathbf{k}_2$, have been neglected since the amplitude of the field modulation is small compared to the static electric field generated by the equilibrium electron density in the QW. We therefore model the field-induced broadening by a Gaussian distribution $g_N(\omega)$ of exciton energies with a full width at half maximum Γ of exciton energies around the center energy ω_{21}^c,[40]

$$g_N(\omega_{21}) = \frac{\sqrt{4\ln 2}}{\Gamma\sqrt{\pi}}\exp\left[-4\ln 2\times\left(\frac{\omega_{21}^c-\omega_{21}}{\Gamma}\right)^2\right]. \tag{5}$$

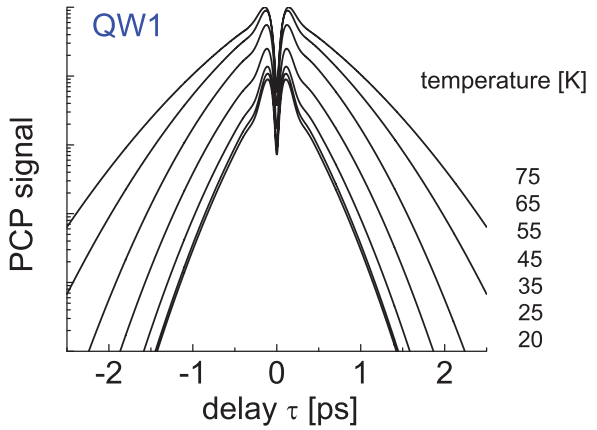

FIG. 10. (Color online) Calculated traces at the spectral position of the X_h heavy-hole exciton in sample QW1 as a function of delay τ at an excitation energy of 2.794 eV and temperatures ranging from 20 to 75 K using Eqs. (6) and (7). E-field-induced inhomogeneous broadening has been considered at this excitation condition.

This inhomogeneous broadening changes the exciton polarization $\boldsymbol{P}_{\mathbf{k}_2}(\tau)$ in Eq. (2) to

$$\begin{aligned}\boldsymbol{P}_{\mathbf{k}_2}(\omega,\tau)_{\text{inh}} \propto \frac{i}{\hbar}\frac{2\sqrt{\pi\,\ln 2}}{\Gamma}\,\mu_{21}^2\exp(i\omega\tau)\\ \times\exp\left(-4\ln 2\frac{\left(\omega_{21}^c-\omega_{21}\right)^2-\gamma_2^2}{\Gamma^2}\right)\\ \times\exp\left(i\,8\ln 2\frac{\gamma_2\left(\omega_{21}^c-\omega_{21}\right)}{\Gamma^2}\right)\\ \times\operatorname{erfc}\left[2\sqrt{\ln 2}\left(\frac{\gamma_2}{\Gamma}+i\frac{\left(\omega_{21}^c-\omega_{21}\right)}{\Gamma}\right)\right]\end{aligned}\quad(6)$$

and function $a_{\mathbf{k}_2-\mathbf{k}_1}$ in Eq. (3) to

$$\begin{aligned}a_{\mathbf{k}_2-\mathbf{k}_1}(\tau)_{\text{inh}} &= \int_0^\infty g_N(\omega_{21})\,a_{\mathbf{k}_2-\mathbf{k}_1}(\tau,\omega_{21})\,d\omega_{21}\\ &= a_{\mathbf{k}_2-\mathbf{k}_1}\left(\tau,\omega_{21}^c\right)\exp\left(-\frac{\tau^2\Gamma^2}{16\ln 2}\right).\end{aligned}\quad(7)$$

Figure 10 shows the calculated traces of QW1 for different temperatures at excitation energy 2.794 eV. The center frequency ω_{21}^c of the inhomogeneously broadened exciton line has been taken from Fig. 6. The inhomogeneous broadening Γ and dephasing rate γ_2 has been mutually adjusted for each temperature until the calculated trace and spectrum show optimum agreement with the experimental trace and spectrum. In addition, parameters a and b have been adjusted to fit the signal suppression at the pulse overlap shown in Fig. 8. The accuracy of the exciton dephasing rates obtained from this two-parameter fit using Eqs. (6) and (7) is better than $\pm 10\%$ (in ps^{-1}) of the values shown in Fig. 7. Similar model calculations have also been applied to QW2 at an excitation energy of 2.794 eV and for laser energy-dependent measurements on QW1 and QW2. The calculated traces and spectra are in very good agreement with the experimental data and were used to determine the exciton dephasing rate and space-charge fields as discussed in Sec. III A.

IV. SUMMARY

We have performed excitation energy and temperature dependent two-beam FWM experiments at low pulse intensity (40 kW/cm^2) on two 10-nm ZnSe QW structures grown on GaAs substrate with different $Zn_{0.9}Mg_{0.1}Se$ barrier thicknesses of 20 (QW1) and 30 nm (QW2). QW2 further contains a 20-nm-thick buffer layer between the barrier and the substrate.

When the exciting laser pulse energy is shifted below the exciton transition energy we observe a redshift of the exciton line and an enhanced exciton dephasing rate. This behavior is attributed to an increasing E-field-induced tilt of the QW band structure due to an increasing density of captured electrons caused by the reduced filling of electron states by excitons and a decreased electron escape rate due to Auger processes by exciton recombination. Due to the reduced barrier thickness in QW1 the captured electron density reveals a stronger electron density increase and exciton redshift with decreasing excitation energy as compared to QW2.

At temperatures below 35 K and laser excitation nearly resonant to the exciton energy the formation of trions significantly compensates the creation of a photorefractive electron density grating. As a result the PCP signal is strongly suppressed leading to a dominating PO signal at temporal pulse overlap. At lower excitation energies increasing space-charge fields tilt the QW band, leading to a reduced trion binding energy and enhanced thermal trion ionization resulting in a strong PCP effect even at low temperature. FWM experiments at 12 K with pulse intensities of 5 MW/cm^2 demonstrate the decrease of the trion binding energy and trion signal intensity with decreasing excitation energy supporting our interpretation. The critical trapped electron density in the QW at which trion dissociation occurs is by a factor of more than 2 reduced in QW2, which is attributed to the insertion of a buffer layer which reduces the density of dislocations within the barrier at which electrons can be trapped.

Because of the thermal dissociation of trions at temperatures above 45 K a significant PCP effect exists in both QW samples even at exciton resonant excitation. Model calculations of the signal traces which are based on the optical Bloch equations considering an E-field-induced inhomogeneous broadening of exciton energies are in good agreement with the experimental exciton traces observed at different excitation conditions.

[1]R. Fiederling, M. Keim, G. Reuscher, W. Ossau, G. Schmidt, A. Waag, and L. W. Molenkamp, Nature (London) **402**, 787 (1999).

[2]P. Grabs, G. Richter, R. Fiederling, C. R. Becker, W. Ossau, G. Schmidt, L. W. Molenkamp, W. Weigand, E. Umbach, I. V. Sedova, and S. V. Ivanov, Appl. Phys. Lett. **80**, 3766 (2002).

[3]A. A. Toropov, Y. V. Terent'ev, P. S. Kop'ev, S. V. Ivanov, T. Koyama, K. Nishibayashi, A. Murayama, Y. Oka, A. Golnik, and J. A. Gaj, Phys. Rev. B **77**, 235310 (2008).
[4]D. Ferrand, A. Wasiela, S. Tatarenko, J. Cibert, G. Richter, P. Grabs, G. Schmidt, L. W. Molenkamp, and T. Dietl, Solid State Commun. **119**, 237 (2001).
[5]M. Fadel and A. A. M. Farag, J. Optoelectronics Adv. Mater. **11**, 571 (2009).
[6]D. W. Parent, A. Rodriguez, J. E. Ayers, and F. C. Jain, Solid-State Electron. **47**, 595 (2003).
[7]O. de Melo, G. Santana, M. Melendez-Lira, and I. Hernandez-Calderon, J. Cryst. Growth **201**, 971 (1999).
[8]H. P. Wagner, S. Tripathy, H. P. Tranitz, and W. Langbein, Phys. Rev. Lett. **94**, 147402 (2005).
[9]H. P. Wagner, S. Tripathy, P. Bajracharya, and H. P. Tranitz, Phys. Rev. B **73**, 85318 (2006).
[10]J. Nukeaw, Y. Fujiwara, Y. Takeda, M. Funato, S. Aoki, S. Fujita, and S. Fujita, Thin Solid Films **334**, 11 (1998).
[11]R. Nicolini, L. Vanzetti, G. Mula, G. Bratina, L. Sorba, A. Franciosi, M. Peressi, S. Baroni, R. Resta, A. Baldereschi, J. E. Angelo, and W. W. Gerberich, Phys. Rev. Lett. **72**, 294 (1994).
[12]T. Elsaesser, J. Shah, L. Rota, and P. Lugli, Phys. Rev. Lett. **66**, 1757 (1991).
[13]L. Rota, P. Lugli, T. Elsaesser, and J. Shah, Phys. Rev. B **47**, 4226 (1993).
[14]R. W. Schoenlein, W. Z. Lin, E. P. Ippen, and J. G. Fujimoto, Appl. Phys. Lett. **51**, 1442 (1987).
[15]W. H. Knox, C. Hirlimann, D. A. B. Miller, J. Shah, D. S. Chemla, and C. V. Shank, Phys. Rev. Lett. **56**, 1191 (1986).
[16]W. S. Pelouch, R. J. Ellingson, P. E. Powers, C. L. Tang, D. M. Szmyd, and A. J. Nozik, Phys. Rev. B **45**, 1450 (1992).
[17]J. Shah, A. Pinczuk, A. C. Gossard, W. Wiegmann, and K. Kash, Surf. Sci. **174**, 363 (1986).
[18]T. Tokizaki, H. Sakai, G. Kogano, and A. Nakamura, Jpn. J. Appl. Phys. **38**, 3562 (1999).
[19]T. Tokizaki, H. Sakai, A. Nakamura, Y. Manabe, S. Hayashi, and T. Mitsuyu, Semicond. Sci. Technol. **10**, 1253 (1995).
[20]D. J. Jang, M. E. Lee, Y. H. Chung, C. S. Yang, and W. C. Chou, Jpn. J. Appl. Phys. **47**, 7056 (2008).
[21]A. Nakamura, T. Mukai, Y. Manabe, and I. Tanahashi, J. Lumin. **76-77**, 120 (1998).
[22]M. Mehendale, W. A. Schroeder, S. Sivananthan, and W. Potz, Phys. Status Solidi B **204**, 113 (1997).
[23]H. P. Wagner and A. Dongol (unpublished).
[24]K. Jeong, J. J. Turek, M. R. Melloch, and D. D. Nolte, Appl. Phys. B **95**, 617 (2009).
[25]K. Jeong, J. J. Turek, M. R. Melloch, and D. D. Nolte, Opt. Commun. **281**, 1860 (2008).
[26]P. Yu, M. Mustata, J. J. Turek, P. M. W. French, M. R. Melloch, and D. D. Nolte, Appl. Phys. Lett. **83**, 575 (2003).
[27]A. Kabir, A. M. Ajward, and H. P. Wagner, Appl. Phys. Lett. **93**, 063504 (2008).
[28]A. Kabir, A. Dongol, X. Wang, and H. P. Wagner, Appl. Phys. Lett. **97**, 251116 (2010).
[29]M. Wörz, E. Griebl, Th. Reisinger, R. Flierl, B. Haserer, T. Semmler, T. Frey, and W. Gebhardt, Phys. Status Solidi B **202**, 805 (1997).
[30]H. P. Wagner, H. P. Tranitz, and R. Schuster, Phys. Rev. B **60**, 15542 (1999).
[31]A. J. Shields, F. M. Bolton, M. Y. Simmons, M. Pepper, and D. A. Ritchie, Phys. Rev. B **55**, R1970 (1997).
[32]L. C. O. Dacal and J. A. Brum, Phys. Rev. B **65**, 115324 (2002).
[33]H. P. Wagner and S. Tripathy, Phys. Rev. B **69**, 125325 (2004).
[34]H. P. Wagner, A. Schatz, R. Maier, W. Langbein, and J. M. Hvam, Phys. Rev. B **57**, 1791 (1998).
[35]H. P. Wagner, A. Schaetz, R. Maier, W. Langbein, and J. M. Hvam, Physica E **2**, 82 (1998).
[36]H. P. Wagner, A. Schatz, R. Maier, W. Langbein, and J. M. Hvam, Phys. Rev. B **56**, 12581 (1997).
[37]S. Tripathy, P. Bajracharya, A. Kabir, and H. P. Wagner, in *Physics of Semiconductors, 28th International Conference on the Physics of Semiconductors, ICPS-28, Vienna, Austria*, AIP Conf. Proc. 893 (AIP, Vienna, 2007), p. 419.
[38]T. B. Norris, X. J. Song, W. J. Schaff, L. F. Eastman, G. Wicks, and G. A. Mourou, Appl. Phys. Lett. **54**, 60 (1989).
[39]A. F. M. Anwar and K. R. Lefebvre, Phys. Rev. B **57**, 4584 (1998).
[40]J. Erland, K.-H. Panke, V. Mizeikis, V. G. Lyssenko, and J. M. Hvam, Phys. Rev. B **50**, 15047 (1994).